Growth and lattice dynamics of Co nanoparticles embedded in Ag: A combined molecular-dynamics simulation and Mössbauer study

Marc Hou* and Mahjoub El Azzaoui
Physique des Solides Irradiés, Case Postale 234, Université Libre de Bruxelles, Campus de la Plaine, Boulevard du Triomphe, B-1050 Brussels, Belgium

Hugo Pattyn, Joris Verheyden, and Gerhard Koops
Instituut voor Kern- en Stralingsfysica, Physics Department, K.U. Leuven, Celestijnenlaan 200D, B-3001 Leuven, Belgium

Guilin Zhang
Shanghai Institute of Nuclear Research, Chinese Academy of Sciences Shanghai 201800, People's Republic of China
(Received 18 January 2000)

We use Mössbauer spectroscopy in combination with atomic scale modeling in order to gather a comprehensive understanding of the growth and the dynamics of cobalt nanoprecipitates in silver. The modeling makes use of classical molecular dynamics in the canonical ensemble by means of the Rahman-Parinello technique. Atomic interactions are governed by an embedded atom model, which is validated for the static Co-Ag interaction by means of a comparison with extended x-ray absorption fine structure measurements and for the dynamical interaction with Mössbauer spectroscopy data. This allows us to identify the cluster size dependent atomic arrangements at the cluster-matrix interface, where strong relaxation takes place. A detailed analysis of the Mössbauer spectra taken at two temperatures after annealing at different temperatures allows us not only to characterize the cluster size dependence of magnetic properties, but also to evidence a possible Ostwald ripening growth mechanism. The mean and interface Debye temperatures are deduced from the Mössbauer spectra and found quite consistent with the model predictions. On this basis, the atomic scale modeling allows us to identify detail of atomic vibrational properties as a function of distance from the cluster center and a discontinuity of the vibration amplitudes at the precipitate-matrix interface is evidenced.

I. INTRODUCTION

Although research over the last decades and particularly in recent years has accumulated a wealth of gross structural and magnetic information on embedded nanoclusters in granular materials, their interfacial and atomic scale properties remain largely unexplored. While the system of Co clusters in a Ag matrix is a prototype granular magnetic material with interesting magnetic properties, we mainly turn our attention in this paper to the lattice dynamics of these embedded clusters, expressed concisely in their Debye temperature, Θ_D. A set of recent experiments seems to show that a deviation from the bulk value of the nanoparticle's Θ_D translates changes in its surface-atomic arrangement. In line with observations of a markedly decreasing Θ_D for (quasi) free nanoclusters, a decrease was also observed in nanoparticles with loose interfaces, such as Fe clusters embedded in oxides through cosputtering,[1] or through chemical deposition,[2] and in nanocrystalline material.[3,4] Conversely for tightly embedded nanoclusters, such as the ones typically prepared by ion implantation, Θ_D seems to depend on the matrix. Mainly rare-gas inclusions have shown this effect, with enhancements much higher than what lattice compression could explain,[5–7] while the same systems also contained loosely embedded particles that did not show the enhancement.[6]

The case of well-embedded metallic nanoparticles, with little or no compression, is still poorly documented. A rare example is that of very small nanoclusters of a soft metal like Sn in a hard Si matrix,[8,9] where the $\beta-\mathrm{Sn}\,\Theta_D$ is clearly enhanced. The case presented here is that of a hard metal inclusion ($\Theta_D^{Co}\approx 400K$) in a rather soft matrix ($\Theta_D^{Ag}\approx 225K$), where a pronounced depression of Θ_D^{Co} is to be expected. We bring this interesting system under experimental investigation at the atomic scale, through the incorporation in the Co clusters of ^{57}Co, the radioactive parent isotope of the ^{57}Fe Mössbauer probe. Similarly, we attempt to model very small Co clusters embedded in Ag by molecular-dynamics simulations, tracing observed changes in Θ_D with cluster size to vibrational amplitudes of individual shells. Such clusters were previously observed experimentally by HRTEM.[10] Co in bulk form has an hcp crystal structure at room temperature, transforming to fcc above 698 K. A bcc phase is found in thin films grown on (110) GaAs.[11] Clusters embedded in Ag however generally seem to have the fcc structure.[10] HRTEM allows the identification of preferential morphologies, such as truncated octahedra with eight hexagonal {111} facets and six square {100} facets.

II. THE SIMULATION METHOD

The classical molecular-dynamics method (MD) is a natural choice to study the temporal evolution of a solid system at the atomic scale. The selection of realistic and well-defined thermodynamic conditions is necessary in order to compare model thermal properties with those of a real system. In the present case, we have to model clusters of Co in a Ag matrix in which it is poorly soluble.

The number N of atoms contained in clusters in the shape

of truncated octahedra with regular hexagonal facets is:[12]

$$N(n)=16n^3-33n^2+24n-6, \quad n\geqslant 3. \tag{1}$$

The smallest regularly shaped truncated octahedral clusters thus contain 201, 586, and 1289 atoms, respectively. In the present paper, substitutional Co as well as clusters containing 405 and 1289 atoms are considered. The smallest cluster displays identical hexagonal facets with unequal edges.

In order to compare the properties of different model systems among them and with experiments, it is necessary—because of the occurrence of inhomogeneities—to allow internal relaxation in the model, keeping macroscopic properties unchanged. This is precisely the aim of the Rahman-Parinnello MD method.[13] In this method, the edges of the simulation box, defined by the vectors $\mathbf{u}_1$, $\mathbf{u}_2$, and $\mathbf{u}_3$, are time dependent and periodic boundary conditions are applied. These three vectors define a matrix $\mathbf{H}$ with a determinant that is just the total volume of the simulation box. The use of periodic boundary conditions is made possible by defining a reduced coordinate system ($\mathbf{q}$), related to the real coordinates by the matrix $\mathbf{H}$ according to

$$\mathbf{r_i}=\mathbf{H}\mathbf{q_i}, \tag{2}$$

where $\mathbf{r_i}$ and $\mathbf{q_i}$ are the real and the reduced coordinates of particle i, respectively. The system can be coupled to a thermal bath[14] and constrained to an external pressure[15] by imposing the equations-of-motion to derive from the following Lagrangian:[16]

$$L=\frac{1}{2}\sum_{i=1}^{N} m_i s^2(\mathbf{H}\dot{\mathbf{q}}_i)^t\left(\mathbf{H}\dot{\mathbf{q}}+\frac{1}{2}Q_A Tr(\dot{\mathbf{H}}^t\dot{\mathbf{H}})+\frac{1}{2}Q_N\dot{s}^2 - U(\{\mathbf{H}\mathbf{q}\})-P_{\text{ext}}\Omega-gk_BT_{\text{ext}}\ln(s)\right), \tag{3}$$

where s and $\dot{s}$ are a time dependent parameter and its first time derivative, respectively, which govern the dynamics of the exchange of energy with the thermal bath at the constant temperature T_{ext}. It is associated with an adjustable inertial factor Q_N. Similarly, the volume Ω is also considered as a dynamical parameter, the variations of which are controlled by a constant external pressure P_{ext}. The associated inertial factor is noted Q_A in Eq. (3) and it can also be adjusted. k_B is the Boltzmann constant and g is a function of the number of degrees of freedom of the system, determined in such a way that the Lagrangian (3) is consistent with the partition function of the canonical ensemble. The Nordsick predictor-corrector method[16] to the fifth order is used in order to solve the equations-of-motion stepwise in time. The MD algorithm makes use of a combination between Verlet neighbor lists, a linked cell method, and the third Newton's law.[17] The interaction potential is deduced from the embedded atom model (EAM).[18] Similarly to other schemes, within the EAM, the total energy of the system is written as

$$E=\sum_i\left\{\sum_{j\neq i}\Phi(r_{ij})+F(\rho_i)\right\}, \tag{4}$$

where $\Phi(r_{ij})$ is a two-body central potential between atoms labeled i and j, and $F(\rho_i)$ is a functional of the electronic density ρ_i at atom i considered as embedded into a host matrix, where the local environment determines ρ_i. In the linear combination of atomic orbitals approximation, ρ_i is fully determined by the local atomic wave functions and the hopping integrals, but their exact determination is unrealistic for complex systems. Therefore, we follow the method suggested by Johnson,[19] according to which F is a function of a power of the separation distances and the functional dependence of F on the electronic density obeys the equation-of-states suggested in Ref. 20. This latter function is chosen for convenience to follow a power-law dependency on the electronic density. The parameters in the power-law dependencies are adjusted in order to match several macroscopic and microscopic properties of the material like the equilibrium condition, the elastic constants, and cohesive and vacancy formation energies. This method is found consistent in cases of elemental solids and alloys for which such quantities are known. It is hardly assessed however in the case of heterogeneous systems and interfaces for which such properties are unknown. This is the case for the nonmiscible Co-Ag system that we consider here. The model parameters of elemental fcc Ag and hcp Co are found in Refs. 21 and 22. The heteronuclear repulsive pair potential is estimated according to Ref. 19, which is somewhat arbitrary and does not fully warrant a sufficient accuracy. Therefore, in what follows we compare, as systematically as possible, our model predictions with other experimental observations. This assessment then allows us to compare the lattice dynamics properties of the clusters, taken from the model system, with experimental ones, derived from Mössbauer spectroscopy. Then, detailed information is gathered from the model, which cannot be reached by presently available experimental methods.

As far as thermal properties are concerned, the simulation box size must be large enough for the effect of the elastic stress induced by the presence of a Co cluster in its center to fall off to zero in the vicinity of the edges. Otherwise, the boundary conditions would induce artifacts. The absence of such artifacts was controlled by comparing the mean-squared thermal vibration amplitude (noted ''msqa'' in what follows) of Ag atoms close to the edges of the box with the msqa determined at the same temperature in a perfect Ag single crystal. For the temperature range considered (0 K–700 K), a box of $16\times16\times16$ lattice units size (16 384 atoms) was sufficient in the case of a truncated octahedral Co cluster containing 405 atoms. A box of $24\times24\times24$ lattice units size (55 296 atoms) was necessary in the case of a Co cluster containing 1289 atoms. The comparison between the cases of the 405 and the 1289 atoms clusters provides qualitative insight into what the size effects on relaxation and cluster dynamics are.

III. COMPARISON WITH EXPERIMENT: VALIDATION OF THE MODEL PARAMETERS

A. Static properties

Co_xAg_{1-x} granular alloys were analyzed at low temperature by extended x-ray absorption fine structure (EXAFS) (Ref. 10) for small Co concentration and accurate distance measurements between first neighbor atoms in different close environments were obtained. At the low concentrations employed, EXAFS provides a first neighbor Ag-Co distance of 2.81 Å, which is significantly smaller than the measured bulk

Ag first neighbor distance 2.88 Å. We first model an Ag box with one Co atom at a substitutional site and relax it to its equilibrium configuration at 0 K. An Ag-Co distance of 2.82 Å is found in good agreement with the mentioned experiment. TEM diffraction shows that Co clusters embedded in an Ag matrix are generally found to have an fcc structure. We also observe that the simulated fcc clusters, containing 405 and 1289 atoms respectively, are energetically stable up to 700 K, the temperature where bulk Co has taken an fcc structure. For the Co-Ag distance at the cluster-matrix interface at 0 K, the simulations predict the same distance as for substitutional Co, 2.82 Å, irrespective of the cluster size, again close to the distance of 2.81 Å, which was measured by EXAFS. In the center of the clusters, simulation predicts a Co-Co first neighbor distance of 2.50 Å at 0 K. Experimentally, distances of 2.49 Å (Ref. 10) and 2.50 Å (Ref. 23) are found at 78 K. At room temperature, the bulk first neighbor distance in hcp Co is 2.50 Å and 2.51 Å in its quenched fcc phase.[24] Hence, as static properties of substitutional cobalt and embedded cobalt clusters are concerned, the agreement between the model and available experimental data is quite satisfactory.

B. Dynamical properties

The mean-squared thermal vibration amplitude of particle i can be estimated by molecular dynamics according to the definition

$$\langle u_i^2 \rangle = \langle [\mathbf{r}_i(t) - \overline{\mathbf{r}}_i]^2 \rangle, \tag{5}$$

where $\mathbf{r}_i(t)$ and $\overline{\mathbf{r}}_i$ are the instantaneous and the mean positions of particle i at time t, respectively.

Over an evolution time of 100 ps, we thus estimated the msqa of a Co atom located substitutionally in Ag and we repeated the procedure at several temperatures between 50 and 700 K.[25] This way, we could fit the temperature dependence of $\langle u^2 \rangle$ to the classical Debye relation, with the Debye temperature Θ_D as a fitting parameter:

$$\frac{1}{3}\langle u^2 \rangle = \frac{3\hbar^2}{M k_B \Theta_D}\left[\frac{1}{4} + \left(\frac{T}{\Theta_D}\right)^2 \int_0^{\Theta_D/T} \frac{x e^x}{e^x - 1} dx\right] \tag{6}$$

with M the mass of the Co atom. The fit yields a value $\Theta_D = 218K$. Based on the existence of the direct relation between the msqa and the Mössbauer recoilless fraction f, we can experimentally assess this prediction by a Mössbauer emission experiment on ^{57}Co, substitutionally located in Ag. f, the chance for the emission of the Mössbauer γ quantum ($E_\gamma = 14.4$ keV) without affecting the phonon spectrum:

$$f = \exp(-k^2 \langle x^2 \rangle) = \exp\left(-k^2 \left\langle \frac{u^2}{3} \right\rangle\right), \tag{7}$$

where $\langle x^2 \rangle$ is the component of the msqa in the direction $\mathbf{k}$ of the γ emission with wave-number k.

Since the intensity of a spectral component in the Mössbauer spectrum is proportional to f of the corresponding site, it is straightforward to fit its experimental temperature dependence to the model and to extract the corresponding Debye temperature. We prepared a source of substitutional Co in Ag by implanting ^{57}Co at room temperature and at low dose, 5×10^{13} cm^{-2}, into a previously deoxidized 5-N Ag foil. No further treatment followed the implantation. We recorded Mössbauer spectra at 100, 200, and 293 K. The fit yielded a Debye temperature of 211(18) K, (Ref. 29) in excellent agreement with the value predicted by the MD model. Was the Mössbauer experiment really performed on substitutional Co? The following set of arguments convinced us. (i) The spectra clearly feature an unsplit line, indicative of a cubic environment such as expected for an impurity on a substitutional site in an fcc lattice. (ii) Its room temperature isomer shift is -0.57 mm s^{-1} [all isomer shifts (IS) are given with respect to the sodiumferrocyamide single-line absorber at room temperature], in agreement with previously observed values for substitutional ^{57}Fe in Ag.[26,27] (iii) Implanting ^{57}Co in similar conditions in Au also yielded a single-line component at -0.72 mm s^{-1}, close again to the literature value for Fe substitutional in Au, -0.70 mm s^{-1}.[27] (iv) The scale of isomer shifts pertaining all sites of ^{57}Fe in Ag extends from -0.57 mm s^{-1} as the most negative value, up to -0.05 mm s^{-1} as the most positive value found in the larger Co nanoparticles (cf. infra). In between, when Co clustering sets in, it shifts steadily to intermediate values. We find the component under discussion at the negative extreme of this scale, which corresponds to the lowest electron density at the ^{57}Fe nucleus, again supporting a substitutional site allocation, where the Co impurity atom is fully coordinated by Ag neighbors. (v) The evolution of the population of this component with concentration matches closely what we expect on statistical grounds for a substitutional site, employing a binomial distribution: from almost 100%, found at the lowest concentration, it decreases to 60 and 15% when the concentration increases to 0.05 and 0.10 at. %, respectively.[28]

We believe to have justified the use of the model for predictions beyond possible experimental observation, though as much as possible grounded on further experimental data. In the next section, Co clusters are modeled with morphologies such as encountered in the HRTEM observations mentioned above. Mean thermal vibration properties are then compared with values derived from Mössbauer spectroscopy data on Co nanoclusters in Ag, whereby we describe in detail their spatial dependence, on the basis of MD simulation results. Alongside this comparison, we extract structural information on the clusters that have formed.

IV. COBALT CLUSTERS EMBEDDED IN SILVER

A. Structural properties

The vibrational properties in the vicinity of the cluster-matrix interface are expected to depend on the stress field, just as they do at a macroscopic solid interface. The first neighbor distance is 2.51 Å and 2.88 Å in fcc, Co and Ag, respectively. This creates a significant mismatch between the two lattices and lattice relaxation is to be expected at the interface. We have analyzed this in detail. We already reported in a previous section that the Ag-Co first neighbor distance, averaged over the whole interface, is consistent with the results of EXAFS measurements at low temperature, as well for the corresponding site as for the substitutional site (2.81–2.82 Å). The lattice relaxation, however, depends on position and temperature. The purpose of the present section

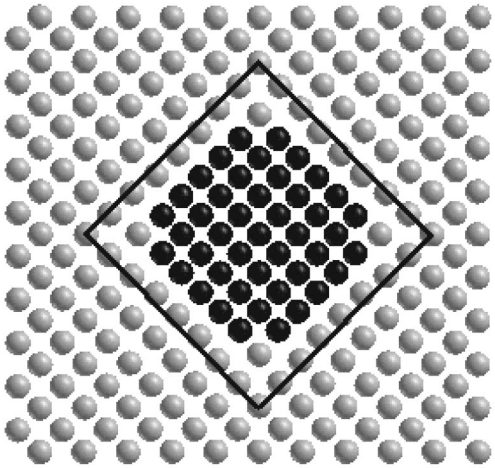

FIG. 1. A {100} slab in the Co_{405} cluster embedded in a Ag matrix. The slab is one monolayer thick. The Co-Ag first neighbor distance depends on the facet orientation. It is the largest in the case of the {111} facets. Ag atoms are represented by grey spheres, Co by black ones. A square is drawn with a solid-straight line to emphasize the distortion of the Ag lattice.

is to show evidence for these dependencies as they come out of the atomic scale computations.

Figure 1 displays a slab in the Co_{405} cluster and the surrounding Ag matrix at 0 K. The thickness is one atomic layer close to the cluster center. Similar slabs indicate inward relaxation of ⟨100⟩ Ag rows parallel to the {100} facets. Beyond the qualitative evidence for strong Ag relaxation, as shown in Fig. 1, a quantitative analysis of the relaxation can be undertaken. At the {111} interface the Co-Ag distance is larger than at the {100} interface. A relaxation is observed corresponding to a mean extension close to 20% with respect to the bulk Ag {111} equidistance and an extension close to 14% as referred to the {100} bulk Ag equidistance, respectively. The relaxation of the Co lattice at the interface is, however, less then 1%, which implies that the interface relaxation is almost fully supported by the Ag matrix. The range of this relaxation, within 1% accuracy, extends no further than the sixth {111} Ag plane from the cluster and to a somewhat shorter distance in the ⟨100⟩ directions. A close look at Fig. 1 indicates that Ag tends to fill the lattice sites that would be occupied by Co atoms in a nontruncated octahedral cluster morphology.

For the larger cluster size the effect of the lattice mismatch is more apparent: the situation is illustrated in Fig. 2. Typical slabs of one atomic layer thickness in the 1289-atom cluster and the surrounding silver matrix are shown at temperatures of 0 K, 100 K, and 700 K. At 0 K, strong distortions are apparent, as in Fig. 1 for the smaller cluster. The tendency for Ag atoms to fill the lattice sites that would be occupied by Co in a nontruncated octahedral morphology is increased and a clear separation between this octahedron and the matrix is apparent. The {111} Ag planes at the interfaces are strongly distorted, with the largest distortion at this interface. Taking the bulk Ag equidistance as a reference, the {111} Ag-Co at the {100} facets is contracted by 20%, while the {111} interfacial distance corresponds to a mean extension of about 25%.

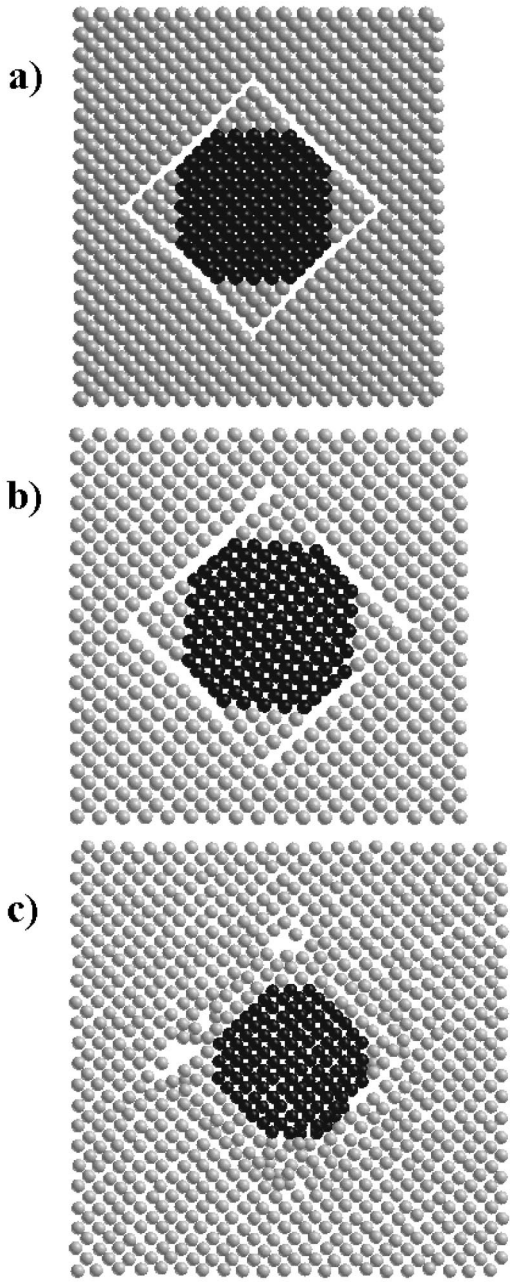

FIG. 2. Three different typical {100} slabs in the Co_{1289} cluster embedded in a Ag matrix. The slabs are each one monolayer thick. (a) T = 0 K, (b) T = 100 K, (c) T = 700 K. Grey sphere: Ag; black ones: Co.

In contrast to what happens for the Co_{405} cluster, the equilibrium configuration at 100 K differs substantially from that at 0 K, as shown in Fig. 2. Indeed, the strong distortions at 0 K are unstable and a small thermal perturbation induces a network of four edge dislocations around the cluster. Their symmetrical arrangement is such that the sum of their Burgers vectors is zero. The residual planar relaxation around the cluster does not have fourfold symmetry and it depends on the exact location of the dislocation cores. The contribution of the dislocations and the interfaces to this relaxation is hardly distinguishable. It should be emphasized that, in contrast with mismatch dislocations at extended boundaries, the dislocation Burger vectors are perpendicular to the interface facets.

At 700 K, Fig. 2(c) shows that the dislocations that remain, but thermal disordering appears in addition, due to the large thermal vibrations of the atoms around their equilibrium positions. In the snapshot displayed, the thermal displacement of some atoms is larger than the slab thickness and they are consequently not seen in the figure. The temperature considered is well below the melting temperature of Ag (1233 K). This disorder may well be a local premelting stage. The melting dynamics is however beyond the scope of the present paper.

Experimentally it is difficult to study the interface in a selective way. We have however tried this with the ^{57}Co probe, taking advantage of the relatively large diffusivity of Co in Ag, compared to that of Co in Co. In a study that was mainly aimed at a determination of the magnetic hyperfine field associated with interface Co atoms,[30] we created Co nanoparticles in a Ag matrix by coevaporating both species and postimplanting the samples with probe atoms. At 4.2 K, the spectral contribution of these probes which had taken up an interface site lies between 30 and 40 % after room temperature (RT) preparation and between 45 and 65 % after 400 °C annealing. This favorable population situation allowed us to deduce the corresponding magnetic fields and Debye temperatures. In order to avoid the complications associated with temperature induced changes in the relative populations of particles from ferromagnetic to superparamagnetic as we increase the measuring temperature (see discussion below), we only collected spectra at the relatively high temperatures, 295, 373, and 473 K, where all nanoparticles already were in the superparamagnetic state.

We used Co concentrations between 3.5 and 22 at. %, corresponding to particle diameters after RT preparation between 7 and 16 nm, as deduced from the probe atom populations,[30] and of only 4 nm for a 15 at. % sample, as we could deduce from fitting the magnetization to a Langevin function. An apparent contradiction in size determination remains unresolved. As was discussed in Ref. 30, the mean interface magnetic hyperfine field increases with the particles size, from 81 to 93 % of the bulk field. It was suggested that this increase corresponds to a larger fraction of Co atoms at {111} interface planes, where they have a relative larger number of Co neighbors, compared to the smaller clusters, where on the average less Co neighbors are to be found. This is confirmed in a recent nuclear magnetic resonance study of Co_xAg_{1-x}.[31]

As far as the corresponding Debye temperatures are concerned, it unfortunately proved futile to try finding a clear dependence. The values ranged between roughly 120 and 240 K, probably depending on the details of the preparation steps and of the formed interfaces. These widely varying values are in qualitative agreement with the findings of the simulations, where we observe that part of the interface strain is relieved by the formation of dislocations, depending on details of the thermal history. The maximal value of the Debye temperature seems to approach that of substitutional Co, which is not unexpected in view of their similar Co-Ag distances. We may also already refer to our discussion in Sec. IV B 1, where it is shown that the Mössbauer spectral components associated with the smaller Co clusters exhibit a large quadrupole interaction, representative of the interface atoms. Figure 3 (bottom) shows this parameter to have no systematic dependence on the annealing temperature, which may result from an unstable interfacial arrangement, again in qualitative support of the simulations.

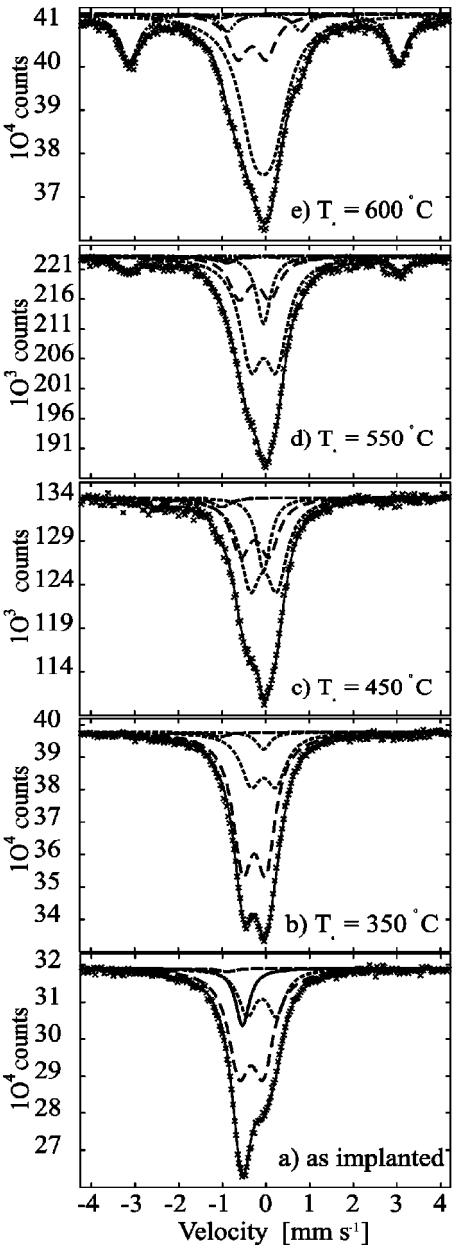

FIG. 3. Annealing temperature dependencies of all parameters extracted from the Mössbauer spectra shown in Fig. 4. The individual components are represented in a similar way as in Fig. 4. Top: Dependence of the spectral intensities of all components on T_a; medium: Dependence of the isomer shift of the components Clust, SPM, and FM on T_a; Top: Dependence of the spectral intensities of all components on T_a; bottom: Dependence of the quadrupole interaction strength of the components Clust and SPM on T_a.

B. Dynamical properties

The present section aims at emphasizing the relation between the vibrational properties of constituent atoms in an embedded cluster, the cluster size, and its interfacial atomic arrangement. In order to tackle this question, we again combine an experimental approach with theoretical simulations.

TABLE I. Mean diameters of Co clusters after implantation of 6 at. %.

As implanted	After 300 °C annealing	After 400 °C annealing
1.4 nm	2.2 nm	3.5 nm

1. Experimental results

An extensive series of temperature-dependent Mössbauer spectra has been collected on carefully deoxidized polycrystalline and single-crystalline Ag samples, implanted with radioactive ^{57}Co probe atoms and postimplanted with stable Co up to 6 at. % in the top 60 nm. The insoluble Co precipitates partly during the implantation and further during an isochronal annealing sequence. The annealing also causes particle growth.

From the ratio of the interfacial to the interior ^{57}Co population, extracted from Mössbauer spectra taken at 4.2 K, and approximating the clusters by spheres, we infer their mean diameters. They are presented in Table I. An x-ray diffraction analysis after 400 °C annealing could only detect the fcc crystal structure, confirming the stability of this phase evidenced by the simulations and HRTEM observations. We have assessed the mean Debye temperature of the clusters formed after annealing steps at $T_a \geqslant 500$ °C through an evaluation of the change of the probability of resonant γ emission at two temperatures, 20 and 200 °C. Some of the results on the polycrystalline material have been succinctly reported in Ref. 29, where the experimental details and a discussion of the analysis method are given. The RT spectra of the single-crystal sample are plotted in Fig. 4. All spectra of both types of samples—a set of several dozens—can be uniquely and consistently analyzed with three main components that belong to the Co nanoparticles, supplemented by two minor ones. Of these minor components, the ''substitutional'' site (denoted *Subst*) with an isomer shift of -0.57 mm s^{-1} has been identified previously in a low-dose experiment, where it was populated for almost 100%. The second minor component is a quadrupole split doublet ($Q3$), close to -1.40 mm s^{-1}, which never exceeds a few percent of the spectral intensity and that has not yet been identified. The three main components are related to the Co clusters themselves: (i) a doublet (Clust), with large quadrupole splitting of around 0.6 mm s^{-1} and IS close to -0.3 mm s^{-1}; (ii) a second quadrupole split doublet (SPM) close to -0.07 mm s^{-1}, with a comparable splitting of around 0.6 mm s^{-1}, and which subdivides above $T_a = 350$ °C in a doublet and a single line; and thirdly (iii) a magnetic sextuplet (FM) with a very similar IS, -0.05 mm s^{-1}.

The precise assignment of these major components is largely based on their hyperfine parameters and on the variation of their spectral intensity with annealing. To this end we present their spectral fractions in the top of Fig. 3, together with their dependence on the annealing temperature. Right after implantation a rather small fraction of Subst remains, but most Co has already started to precipitate out: a smaller part forms SPM, the major part forms Clust. At $T_a = 350$ °C, the remaining fraction Subst precipitates completely, thereby feeding both types of clusters, SPM and Clust. A further increase in T_a causes a gradual transition from the Clust status to the SPM one, followed at still higher

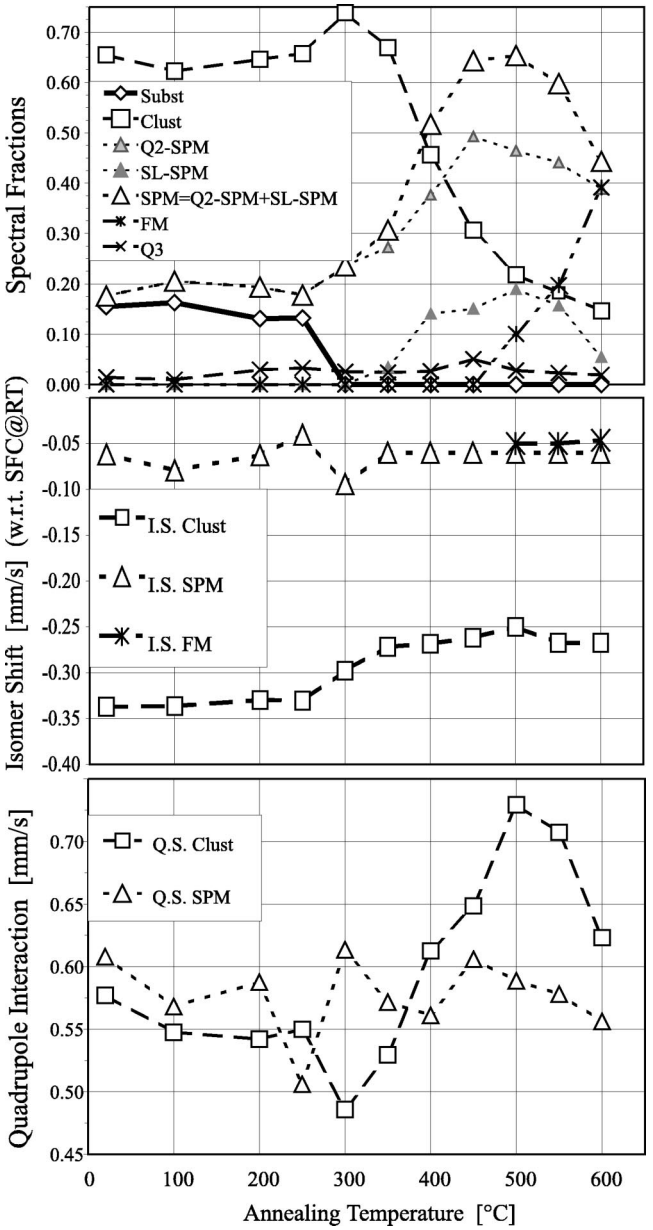

FIG. 4. Mössbauer spectra of the single-crystal sample, collected as a function of annealing temperature T_a. (a) As implanted, (b) 350 °C, (c) 450 °C, (d) 550 °C, and (e) 600 °C. The experimental data points are displayed, together with the overall fit, being the sum of the individual components. The matter are represented by a full line for Subst, a dashed line for Clust, a dotted line for SPM and a dashed and double dotted line for FM.

T_a, close to 500 °C, by a transition from SPM to FM essentially, while Clust starts leveling off. In between, we observed the need to fill in the center of the SPM doublet fraction with a certain amount of single line.

A better understanding of the meaning of the site assignment and of cluster growth is gained by considering at first the behavior of the SPM fraction. It has already partly formed during the implantation itself, which at the high doses employed causes an important radiation enhanced diffusion of the solute atoms. Once the annealing temperature $T_a = 300$ °C is exceeded, where the remaining solute atoms (Subst) become mobile, it grows further either through ab-

sorption of Co atoms from Clust or through transformation of Clust to SPM. At still higher annealing temperatures this fraction gives way to the ferromagnetic one FM, thereby leaving the IS or electron density almost unchanged. Indeed the IS of FM, -0.05 mm s^{-1}, is slightly more positive than that of SPM, which is natural for larger Co particles, where the probe atoms on the average feel little Ag presence and an almost pure Co environment. It is also already close to the value in bulk Co, -0.04 mm s^{-1}.[32] This is what is expected because the SPM-FM transformation is in a way only accidental, corresponding to a freezing in at the measuring temperature of the magnetic moment of the larger clusters within the timeframe of the Mössbauer spectroscopy employed, as will be shown below. Initially the SPM fraction exhibits a quadrupole splitting, stemming from the strong deviation from cubic symmetry of the larger fraction of Co atoms at the particles interface, such as encountered in tiny particles. The need at higher T_a to ''fill the center'' of this spectral component by a single-line component (SL-SPM) with the same IS is readily understood by a diminishing interface contribution due to the subsequent growth of the particles. Its presence supports our identification of the SPM component. The faster decay at $T_a = 600\,^\circ$C of the SL-SPM part compared to the $Q2$-SPM part, may be indicative of an Ostwald ripening process,[33] where individual atoms migrate from the SPM particles boundary to the FM ones. The remaining SPM particles then become smaller and on the average deviate more again from cubic symmetry.

The strength of the quadrupole interaction further supports this picture where SPM is attributed to the smallest Co clusters, since surfaces and interfaces typically exhibit values of this magnitude.[34] The FM component has a magnetic hyperfine field of 33.3(4) T, which is however significantly larger than literature values for hcp Co [31.6 T (Ref. 35)] and fcc Co [31.2 T (Ref. 36)] than a value previously observed in Co clusters in Ag, 30.5 T.[30] In the latter case however it was argued[37] that the reduction may have been caused by the incorporation of a fraction of Ag atoms in these Co clusters. A marked difference between the present single-crystal data and the previous ones on polycrystalline Ag is the total absence of this FM fraction below $T_a = 450\,^\circ$C in the former case. In the polycrystalline material, annealing at T_a as low as 275 °C already induced a sizeable fraction of FM clusters, around 10% of the spectral intensity. Solute segregation at subgrain boundaries, followed by growth into relatively large particles, is probably the cause of this phenomenon, although a preliminary orientational image microscopy picture of the sample did not reveal a dense boundary network.

Clust, the most prominent component, is the least clearly identifiable. Most notable is its prominence right after the implantation, even increased at $T_a = 300\,^\circ$C, where the remaining part of *Subst* precipitates. Its IS and quadrupole splitting dependence on T_a, together with that of the other cluster related components, is shown in Fig. 3 (bottom and middle). The position of its IS, between Subst and both SPM and FM, clearly points to an environment with more Ag neighbors. Its quadrupole interaction corresponds to strong deviations from cubic symmetry.

We tentatively identify this component with small Co clusters, still dispersed with Ag atoms, probably similar to the diluted, fractal-like ''precursor'' precipitation stage, which was observed in Co(Cu),[38] or the linear, wirelike structure, observed in EXAFS measurements on Co codeposited with Ag at low temperature.[23] Between $T_a = 300$ and 500 °C, its fraction exchanges with that of SPM and the ensuing rearrangement seems to expel some of the Ag, as manifested by the concurrent shift in IS. This may be indicative of the transition from a more linear to a more three-dimensional structure.

The following discussion of the lattice dynamical and related information is based on the polycrystalline data, where the analysis is easier. This is because at the highest T_a (i) the FM fraction is more strongly populated and (ii) the SPM has been reduced to zero, which is still not the case at $T_a = 600\,^\circ$C for the single-crystal sample. We have access to the mean Θ_D value of one of the spectral components through the ratio of its normalized relative spectral area, measured at 20 and 200 °C.

In order to avoid any possibly modification in the particle structure or in the particles size distribution during the long measuring periods at 200 °C, we only consider them after annealing steps above 500 °C.

A change that we cannot avoid, however, is the transition of the smaller ones of the RT FM fraction to the higher end of the SPM fraction at 200 °C. Whether this happens and to what extent depends on the overall size distribution of the particles. Consequently, the observation of the phenomenon will at the same time provide a certain window on that size distribution. The rather narrow boundary region between a magnetic Co particle revealing itself in a ^{57}Co(Fe) Mössbauer spectrum as either SPM or FM lies at a volume V given by $KV \approx 2.3 \times k_B T_b$, where K is the anisotropy energy density and T_b is the transition or ''blocking'' temperature. If K equals twice the bulk Co value, 1×10^5 J m^{-3}, this would correspond to particles of a diameter of about 5.6 nm at 20 °C and 6.6 nm at 200 °C. For Co clusters formed by coevaporating Co and Ag at RT, we found $K = 5 \times 10^4$ J m^{-3} for particles of mean diameter 22 nm (through a comparison of the coercive force, measured at 10 and 290 K) and 6×10^5 J m^{-3} for 2.2 nm ones (through a magnetization measurement yielding the size, combined with a determination of T_b). Polymer isolated fcc Co particles of diameter 4.4 and 1.8 nm were recently reported with K values of 4×10^5 J m^{-3} and 3×10^6 J m^{-3}, respectively.[39] An eightfold increase in K, which thus seems quite possible, would reduce the critical diameter by only a factor of 2.

$T_a = 650\,^\circ$C is an easy and convenient starting point for this analysis, because the SPM fraction has been reduced to null by now, even at 200 °C. Here we deduce Θ_D directly from the intensity ratio of the FM fraction, yielding 410(20) K, compatible with the bulk Co value. We suppose that this remains the value for the FM fraction, also after the lower T_a. It indeed appears appropriate to employ bulk property values for that part of the particles distribution exceeding $d = 6.6$ nm, as supported by observations in Ref. 1. At the lower annealing temperatures, we need to evaluate α, the fraction of the total size distribution that makes the transition, i.e., the fraction between the V_{20} and V_{200}, the critical volumes at a measuring temperature of 20 and 200 °C, respectively.

We obtain α as a function of T_a from the normalized spectral intensities, I, of the component FM by keeping the

TABLE II. Θ_D of (Clust + SPM) and size distribution as a function of T_a.

	$T_a = 520\,^\circ$C	570 °C	620 °C	650 °C
Θ_D (Clust + SPM)	252(30) K	286(30) K	314(30) K	370(40) K
Mean diameter (Clust + SPM) [from relation (11)]	2.7 nm	3.3 nm	3.8 nm	4.9 nm
Fraction (Clust + SPM + FM) $<V_{20}$	79.9%	67.6%	34.0%	28.0%
α = Fraction (Clust + SPM + FM) $>V_{20}$ and $<V_{200}$	3.3%	2.4%	2.2%	0.0%
Fraction (Clust + SPM + FM) $>V_{200}$	12.6%	26.4%	61.2%	60.6%

ratio of the recoilless fraction at the two temperatures equal to that measured after $T_a = 650\,^\circ$C:

$$\left(\left[\frac{f_{20\,^\circ\mathrm{C}}}{f_{200\,^\circ\mathrm{C}}}\right]_{FM}\right)_{T_a} = \left(\left[\frac{f_{20\,^\circ\mathrm{C}}}{f_{200\,^\circ\mathrm{C}}}\right]_{FM}\right)_{T_a=650\,^\circ\mathrm{C}} \left(\frac{(1-\alpha)_{T_a} I_{20\,^\circ\mathrm{C}}}{I_{200\,^\circ\mathrm{C}}}\right)_{FM}. \tag{8}$$

Having deduced α in that way, we use it to increment the 200 °C intensity of the smaller clusters, whereby we sum up the spectral intensities of both Clust and SPM. This way we calculate their average Θ_D from the relation:

$$\left(\left[\frac{f_{20\,^\circ\mathrm{C}}}{f_{200\,^\circ\mathrm{C}}}\right]_{CS}\right)_{T_a} = \left(\frac{I_{20\,^\circ\mathrm{C}}}{(1+\alpha)_{T_a} I_{200\,^\circ\mathrm{C}}}\right)_{CS}, \tag{9}$$

where CS refers to the cumulative contributions of Clust and SPM.

The results are presented in Table II. In order to make our information on the size distribution more quantitative, we derive absolute populations by dividing the spectral intensities by the corresponding f fractions, assuming Θ_D for the transferred fraction to be equal to Θ_D of Clust + SPM + FM. These results put the following observations into relief:

(1) The smaller Co nanoparticles that are formed by the lower annealing temperatures exhibit a Debye temperature that is markedly lowered, down to 252(30) K, compared to the value of the largest ones, 410(20) K. One may expect a further decrease for even smaller particles, such as the ones of $\tilde{d} \approx 3.5$ nm, formed after $T_a = 400\,^\circ$C. It indicates that Θ_D comes quite close to the value observed for Co, which is fully coordinated by Ag neighbors at substitutional sites. Both the experimental situation and the simulation results agree very well in this respect.

(2) The value obtained after $T_a = 650\,^\circ$C pertains in fact only to the Clust fraction, since the population of SPM is zero here. The Θ_D value of these smaller clusters is nevertheless astonishingly large, 370(40) K. This is especially so if we compare it on the one hand to the values given above for the combined Clust + SPM, at the lower T_a, and on the other hand to a value $\Theta_D < 300$ K, which we obtained recently in a sample implanted to the low concentration of 0.14 at. %, where this one is the only cluster related site.[40] A tentative interpretation relies in the expulsion of Ag from this ''precursor'' cluster (*vide supra*), such as seems to occur at higher temperatures, which would harden these particles in comparison to a rather loose structure at lower concentrations and temperatures.

(3) The fraction α remains astonishingly small, meaning that the window in the size distribution between the diameters of approximately 5.6 and 6.6 nm is essentially empty. It implies that during annealing above 520 °C, single Co atoms dissolve from the smaller Co particles and migrate to the FM fraction, without particles in the intermediate size range being formed. This is what happens in an Ostwald ripening process.[33] The gap in the size distribution indicates a clear example of a bimodal size distribution, where the FM part gradually grows and simultaneously shifts to larger radii, suggesting that the part α is only the lower end tail of the distribution of the larger particles.

Figure 5 gives a sketchy representation of how the size distribution may look like and further evolve as a function of annealing. The areas respect the fractional contributions and the dashed-central part corresponds to the size ''window''

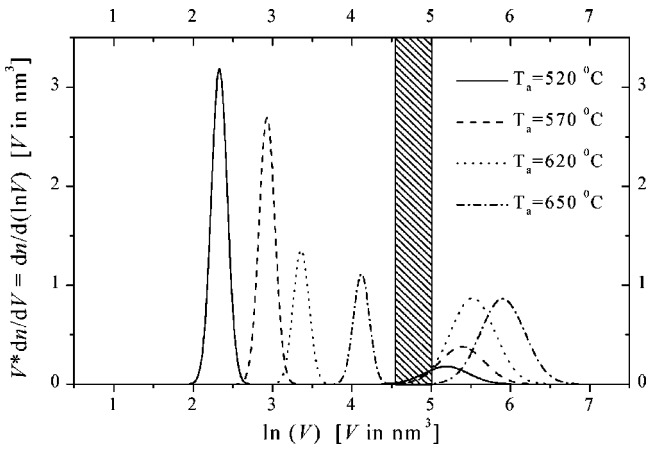

FIG. 5. Schematic representation of a possible Co cluster size distribution and its evolution as a function of T_a. The lower limit of the dashed area, corresponding to a diameter of 5.6 nm, indicates the critical volume of a magnetic cluster with anisotropy energy density $1 \times 10^5 < \mathrm{J\,m^{-3}}$, below which it will be observed in a Mössbauer experiment at 20 °C as superparamagnetic and ferromagnetic above. The upper limit holds for a measuring temperature of 200 °C.

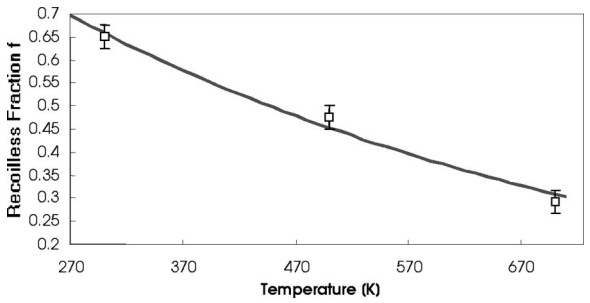

FIG. 6. Fit to the Debye function of the average msqa of Co in the embedded 1289-atom cluster, calculated at 300, 500, and 700 K. The fit yields a value Θ_D of 267 K.

between the blocking temperatures of 20, respectively, 200 °C. A very recent study of Co clustering in Ag, albeit at higher concentrations, also shows evidence of a bimodal size distribution.[31]

2. Simulation results

For the 405 atoms cluster, we found an average Debye temperature for the Co atoms of $\Theta_D = 230$ K,[25] which is close to, though higher than, the value found in the case of isolated substitutional atoms. In the case of the 1289-atoms cluster, we obtain an average Debye temperature by fitting the Debye relation [expression (8), given above] to $\langle u^2 \rangle$, calculated at 300, 500, and 700 K, as shown in Fig. 6. A value of $\Theta_D = 267$ K results, which is clearly higher than in the case of the smaller cluster.

The mean cluster Debye temperature thus appears to be increasing with the cluster size, which is in agreement with the results of Mössbauer spectroscopy measurements. At this point it is tempting to try to compare these calculated values with the experimental ones in order to check the corresponding cluster sizes, through a functional dependence between Θ_D and d, the cluster diameter. To this end, we combine appropriate asymptotic values with the calculated Debye temperatures of the Co clusters (405 and 1289 atoms, corresponding to an estimated d of 2.1 and 3.0 nm, respectively, approximating the clusters by spheres and employing the bulk Co density).

At the lower size end, we assume an asymptotic Θ_D value of 211 K, which is the one calculated for a single substitutional Co atom, while at the higher end we take the bulk Co value of 395 K. We approximate this functional dependence by an *ad hoc* sigmoidal relationship, of the following form:

$$\Theta = \Theta_{\max} + \frac{\Theta_{\min} - \Theta_{\max}}{1 + e^{(d-d_0)/w}}, \tag{10}$$

where Θ_{max} and Θ_{min} are 395 and 211 K, respectively, and where d_0 and w are fitted as 3.6 and 0.68 nm, respectively. From this tentative relationship, we estimate values ranging from 2.7 to 4.9 nm for the mean diameter of the clusters belonging to the lower part of the bimodal size distribution (i.e., the fraction Clust + SPM).

This is displayed in Fig. 7, while the extracted d values are reproduced in the third row of Table II. The lower value of 2.7 nm seems to fit rather well in the cluster growth trend, which we extracted directly from Mössbauer spectroscopy

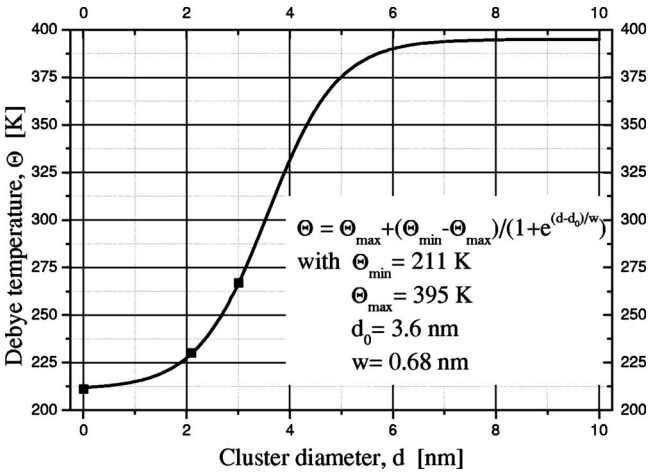

FIG. 7. Relationship between the Debye temperature Θ_D and the mean diameter d of the Co clusters, approximated by an *ad hoc* sigmoidal function, with asymptotic values 395 K for the largest clusters and 211 K for the smallest ones (a single atom). The squares represent the calculated values for substitutional Co, the 405-atom cluster and the 1289-atom cluster.

(Table I), taking into account that the present value discounts the contribution from FM. The larger value of 4.9 nm being rather close to the lower limit, 5.6 nm, of our ''observation window,'' seems to indicate on the other hand that 1×10^5 J m^{-3} is an overestimation of the anisotropy energy density K of these Co clusters.

The calculated Debye temperatures, which we discussed above, are derived from the overall temperature dependence of the msqa. It is worthwhile to compare the temperature dependencies of the two clusters in more detail. Figure 8 displays the msqa of the two clusters and the Ag matrix in which they are embedded. Consistently, the msqa values of the silver matrix are found the same, within statistical error, in both cases and it is also the same as computed for a pure Ag single crystal. This confirms that the size of the simulation box is sufficiently large. The Co clusters msqa values differ and the divergence increases with increasing temperature. The temperature dependence for the 1289-atoms cluster is less pronounced, which explains the higher Debye tem-

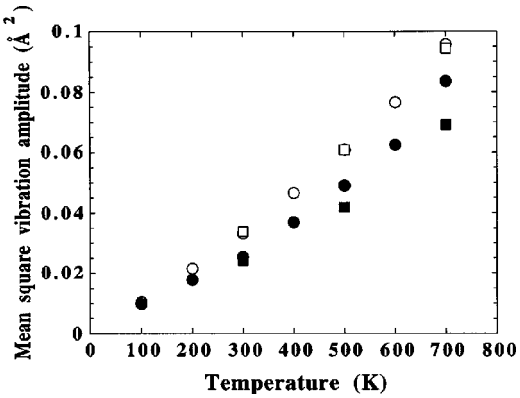

FIG. 8. Mean-squared thermal vibration amplitude averaged over all the atoms in the Co clusters (black symbols) and in the Ag matrix (open symbols). Circles: Co_{405} results, squares: Co_{1289} results.

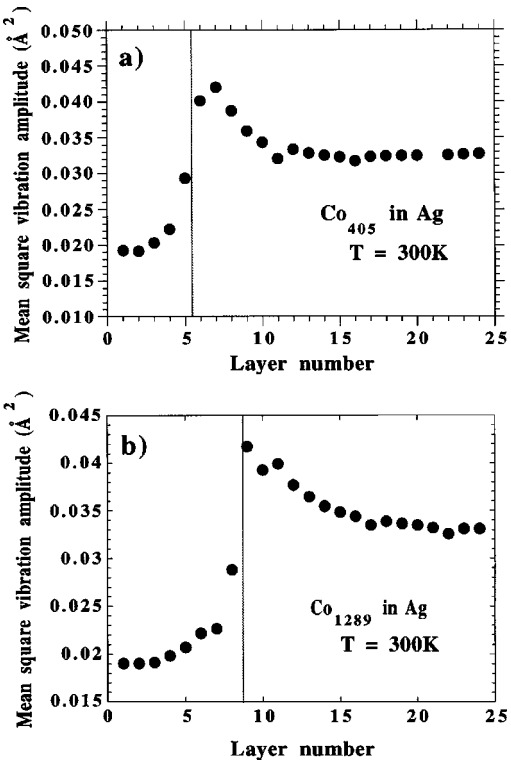

FIG. 9. Mean-squared thermal vibration amplitude at $T=300$ K estimated layer by layer from the center of the cluster. The layers are self-similar to the cluster surface and the dotted line represents the interface position between the cluster and the matrix. (a) Co_{405} results, (b) Co_{1289} results.

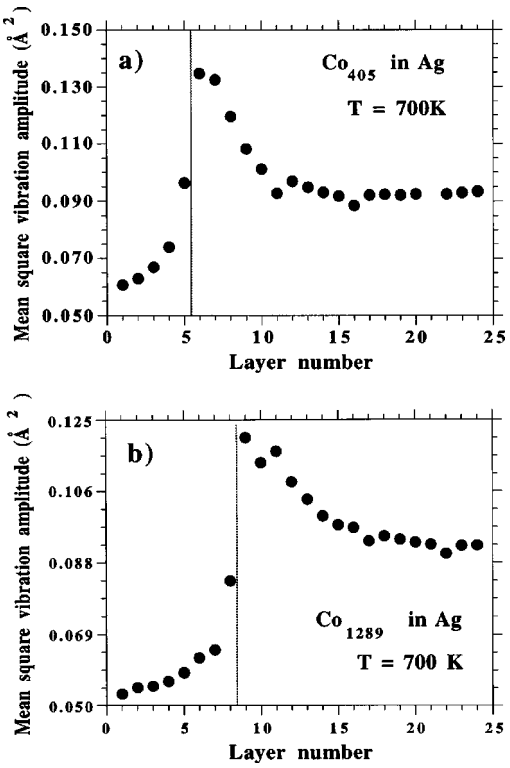

FIG. 10. Same as Fig. 9 at a temperature $T=700$ K.

perature. The remaining question is now to try to identify the physical reasons for this divergence.

In order to answer this question, the msqa is analyzed, not only as a function of temperature, but also as a function of the distance from the cluster center. Therefore, the msqa is evaluated layer by layer, whereby each layer is self-similar to the cluster surface. The results at $T=300$ K are compared in Fig. 9 for the 405- and the 1289-atoms clusters. A vertical line references the Co-Ag interface. In both cases, there is a strong enhancement of the msqa at the interface for both Co and Ag. The discontinuity at the interface in the msqa is a function of the distance from the center of the cluster and is due to the difference in the force constants for Co and Ag. It is striking that the msqa of both interfacial Co and Ag are similar, though not identical, for the 405- and the 1289-atoms cluster. It is only weakly cluster size dependent. This may be related to the fact that dislocations rather than distortions accommodate the lattice mismatch at the interface of the largest clusters. In such a way, the interface relaxation can be similar in both cases. This result is confirmed at the highest temperature considered, as attested by the Fig. 10, which is the same as Fig. 9 but for a temperature of 700 K. The same conclusion is found at all temperatures investigated. This interfacial enhancement is typical of all solid systems where atomic scale relaxation occurs at the interface. It is found however in Fig. 11 that the msqa at the center of the cluster is size dependent at high temperature.

With these elements, it is possible to single out two reasons why the mean Debye temperature is size dependent. First, the surface to volume ratio decreases with increasing cluster size. Hence, the relative number of atoms contributing large values to the msqa is a decreasing function of the cluster size. Second, when the clusters are small, the interface enhancement effect of the msqa extends to the core and in the core it is larger than otherwise. This effect decreases with increasing cluster size and decreasing temperature. This is attested by the plateau value close to the center observed in the 1289-atoms cluster in Fig. 9(b), which does not take place in Fig. 9(a) displaying the 405-atoms cluster results. This plateau disappears at higher temperatures, as shown in Fig. 10(b). Finally, it is worthwhile to notice that this conclusion is drawn in the case of compact clusters with sharp

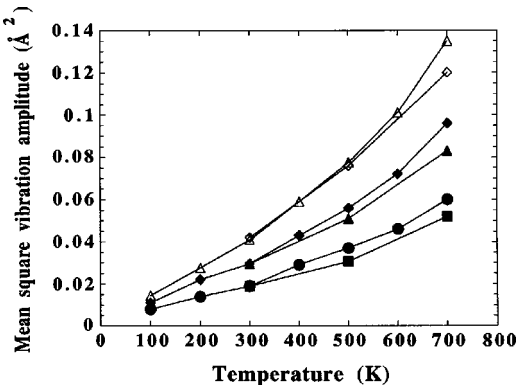

FIG. 11. Mean-squared thermal vibration amplitude in distinct areas as a function of the temperature. Black squares: in the center of the Co_{1289}; black circles: in the center of the Co_{405} cluster; black triangles: Co at the Co_{1289}/Ag interface; black diamonds: Co at the Ag/Co_{405} interface; open diamonds: Ag at the Ag/Co_{1289} interface; open triangles: Ag at the Ag/Co_{405} interface. The solid lines are plotted to guide the eye.

interfaces. Such sharp interfaces are realistic in the case of nonmiscible systems and the model is consistent with the HRTEM results in Ref. 10.

V. CONCLUSION

The present paper is an illustration of Mössbauer spectroscopy and molecular-dynamics bridging, in an efficient way, of the atomic and the microscopic scales, and the duration of a thermal vibration to that of the growth of a precipitate. We could demonstrate that the results of both approaches are complementary to a large extent. The fact that Co and Ag are not miscible precludes the Co-Ag interaction to be modeled on equilibrium macroscopic alloy properties. An alternative could be to fit a classical model on *ab initio* predictions for nonequilibrium systems. In the present case however, atomic scale experimental data are made available by HTREM and EXAFS measurements, which allow an assessment of the equilibrium model in its static properties. This is however not sufficient for molecular dynamics and Mössbauer spectroscopy was necessary to assess the dynamical modeling of substitutional Co. Then, MD could be used to provide insight in the detailed atomic configuration dependence on the size of the Co precipitate and on the temperature of the system.

When the cluster is small enough, the relaxation, always taken up for the major part by the Ag matrix, takes the form of lattice distortions. These turn out to be unstable for the larger cluster and shrink into a dislocation system.

The trend, observed by Mössbauer spectroscopy, for the mean cluster Debye temperature to increase with cluster size, is confirmed by MD, as well as the enhancement of the thermal vibration amplitude at the interface of the precipitates. This consistency between Mössbauer spectroscopy and MD allowed us to use MD for a better understanding of the details of the vibrational properties and it was found that the thermal msqa increases from the center of the cluster towards the interface. There a discontinuity takes place, related to the different elastic properties of Ag and Co.

Beyond the short term atomic scale information gathered with MD, the detail of the Mössbauer spectra allowed us not only to identify the size dependence of the magnetic properties of the Co precipitates, but also to gather insight in the temperature activated growth mechanism of Co clusters. Evidence is found for the generation of a bimodal cluster size distribution, with the larger sizes being promoted by an increase in annealing temperature, the growth occurring via atomic Co diffusion, suggesting an Ostwald ripening mechanism.

We found no evidence in this paper for a coupling between the magnetic and the structural properties of the cluster, although it cannot be excluded. To our knowledge, no theory (both classic and *ab initio*) on which MD models are grounded nowadays account for such a coupling, leaving, possibly, a challenging problem for the future.

ACKNOWLEDGMENT

This work was supported by the PAI/IUAP Contract No. 4/10 and by a Flemish-Chinese bilateral collaboration, Project No. BIL/98/07.

*Corresponding author. Electronic address: mhou@ulb.ac.be

[1] J. R. Childress, C. L. Chien, M. Y. Zhou, and Ping Sheng, Phys. Rev. B **44**, 11 689 (1991).
[2] I. P. Suzdalev, J. Radioanal. Nucl. Chem. **190**, 279 (1995).
[3] J. Jiang, S. Ramasany, R. Birringer, U. Gonser, and H. Gleiter, Solid State Commun. **80**, 525 (1991).
[4] Y. H. Zhao and K. Lu, Phys. Rev. B **56**, 14 330 (1997).
[5] C. J. Rossouw and S. E. Donnelly, Phys. Rev. Lett. **55**, 2960 (1985).
[6] K. Milants, P. Hendrickx, J. Verheyden, T. Barancira, W. Deweerd, H. Pattyn, S. Bukshpan, F. Vermeiren, and G. Van Tendeloo, Phys. Rev. B **55**, 2831 (1997).
[7] Giuseppe Faraci, Agata R. Pennisi, and Jean-Louis Hazemann, Phys. Rev. B **56**, 12 553 (1997); G. Faraci, S. La Rosa, A. R. Pennisi, S. Mobilio, and G. Tourillon, *ibid.* **43**, 9962 (1991).
[8] L. K. Nanver, G. Weyer, and B. Deutch, Phys. Status Solidi A **61**, K29 (1980).
[9] Thaddie Barancira, Ph.D. thesis, K.U.Leuven, 1999 (unpublished).
[10] V. Dupuis, J. Tuaillon, B. Prével, A. Perez, P. Mélinon, G. Guiraud, F. Parent, L. B. Steren, R. Morel, A. Barthlmy, A. Fert, S. Mangin, L. Thomas, W. Wernsdorfer, and B. Barbara, J. Magn. Magn. Mater. **165**, 42 (1997); V. Dupuis, J. Tuaillon, B. Prével, A. Perez, and P. Mélinon, Z. Phys. D: At., Mol. Clusters **40**, 155 (1997).
[11] G. A. Prinz, Phys. Rev. Lett. **54**, 1051 (1985).
[12] R. van Hardeveld and F. Hertog, Surf. Sci. **15**, 189 (1969).
[13] M. Parinnello and A. Rahman, J. Appl. Phys. **52**, 7182 (1981).
[14] S. Nosé, J. Chem. Phys. **81**, 511 (1984).
[15] H. C. Andersen, J. Chem. Phys. **72**, 2384 (1980).
[16] A. Nordsick, Math. Comput. **16**, 22 (1962).
[17] See, e.g., *Computer Simulation of Liquids*, edited by Allen and Tildesley (Oxford Science, Oxford, 1987).
[18] M. S. Daw and M. I. Baskes, Phys. Rev. Lett. **50**, 1285 (1983).
[19] R. A. Johnson, Phys. Rev. B **41**, 9717 (1990).
[20] J. H. Rose, J. R. Smith, F. Guinea, and J. Ferrante, Phys. Rev. B **29**, 2963 (1984).
[21] M. I. Haftel, Phys. Rev. B **48**, 2611 (1990).
[22] D. J. Oh and R. A. Johnson, J. Mater. Res. **3**, 471 (1988).
[23] J. R. Regnard, J. Juanhuix, C. Brizard, B. Dieny, and B. Mevel, Solid State Commun. **97**, 419 (1996).
[24] A. Taylor, *X-ray Metallography* (Wiley, New York, 1961).
[25] M. El Azzaoui, M. Hou, H. Pattyn, J. Verheyden, W. Deweerd, G. Koops, and G. L. Zhang, Nanostruct. Mater. **12**, 299 (1999).
[26] B. D. Sawicka, Radiat. Eff. **48**, 25 (1980).
[27] N. N. Greenwood and T. C. Gibb, *Mössbauer Spectroscopy* (Chapman and Hall Ltd., London, 1971), p. 90.
[28] J. Verheyden, G. L. Zhang, J. Dekoster, A. Vantomme, W. Deweerd, K. Milants, T. Barancira, and H. Pattyn, J. Phys. D **29**, 1316 (1996).
[29] H. Pattyn, J. Verheyden, W. Deweerd, G. E. J. Knoops, G. L. Zhang, M. El Azzaoui, and M. Hou, Hyperfine Interact. **120/121**, 291 (1999).
[30] J. Verheyden, S. Bukshpan, J. Dekoster, A. Vantomme, W. Deweerd, K. Milants, T. Barancira, G. L. Zhang, and H. Pattyn, Europhys. Lett. **37**, 25 (1997).

[31] Yu. G. Pogorelov, G. N. Kakazei, J. B. Sousa, A. F. Kravets, N. A. Lesnik, M. M. Pereira de Azevedo, M. Malinowska, and P. Panissod, Phys. Rev. B **60**, 12 200 (1999).
[32] S. M. Qaim, Proc. Phys. Soc. Jpn. **90**, 1065 (1967).
[33] H. Schroeder, P. F. P. Fichtner, and H. Trinkhaus, *Fundamental Aspects of Rare Gases in Solids* (Plenum Press, New York, 1981), Chap. 2.
[34] H. Pattyn, P. Hendrickx, and S. Bukshpan, in *Fundamental Aspects of Inert Gases in Solids*, NATO ASI Series, Series B: Physics, edited by S. E. Donnelly and J. H. Evans (Plenum Press, New York, 1991), Vol. 279, pp. 243–250.
[35] G. J. Perlow, C. E. Johnson, and W. Marshal, Phys. Rev. **140**, A875 (1965).
[36] A. M. Portis and A. C. Gossard, J. Appl. Phys. Suppl. **31**, 2055 (1961).
[37] J. Verheyden, Ph.D. thesis, K.U. Leuven, 1998 (unpublished).
[38] W. Wagner, Acta Metall. Mater. **38**, 2711 (1990); W. Wagner, Z. Metallkd. **80**, 873 (1989); Xiaodan Jiang, W. Wagner, and H. Wollenberger, *ibid.* **82**, 192 (1991).
[39] J. P. Chen, C. M. Sorensen, K. J. Klabunde, and G. C. Hadjipanayis, Phys. Rev. B **51**, 11 527 (1995).
[40] To be published.